ACS Catalysis

Research Article

pubs.acs.org/acscatalysis

Lanthanum Oxide-Modified Cu/SiO_2 as a High-Performance Catalyst for Chemoselective Hydrogenation of Dimethyl Oxalate to Ethylene Glycol

Xinlei Zheng, Haiqiang Lin,* Jianwei Zheng, Xinping Duan, and Youzhu Yuan*

State Key Laboratory of Physical Chemistry of Solid Surfaces and National Engineering Laboratory for Green Chemical Production of Alcohols-Ethers-Esters, College of Chemistry and Chemical Engineering, Xiamen University, Xiamen 361005, China

Supporting Information

ABSTRACT: Several lanthanum oxide-modified Cu/SiO_2 (La-Cu/SiO_2) catalysts synthesized by urea-assisted gelation and postimpregnation were used for the vapor-phase chemoselective hydrogenation of dimethyl oxalate (DMO) into ethylene glycol (EG). The 1.0La-Cu/SiO_2-*u* catalyst with 1.0 wt % La loading was found to have the highest activity, whereas the catalyst with higher La loading at 3.0 wt % adversely affected the deterioration of catalytic activity. H_2-TPR results revealed that strong interactions between La promoters and Cu species substantially changed catalyst reducibility and made some Cu^{2+} species on catalyst precursors difficult to be reduced. Several positive variations induced by the introduction of La were confirmed by in situ XRD, N_2O chemisorption, H_2-TPD, X-ray Auger electron spectroscopy, and in situ FT-IR of chemisorbed CO. These variations included increased Cu metallic dispersion, improved ability for H_2 activation, elevated surface concentration of Cu^+ species, and enhanced stability of catalyst nanostructure. The formation of unique Cu−O−La bonds between LaO_x and cupreous species located at interfacial sites was presumably responsible for the improved catalytic performance and stability of La-Cu/SiO_2-*u* catalyst.

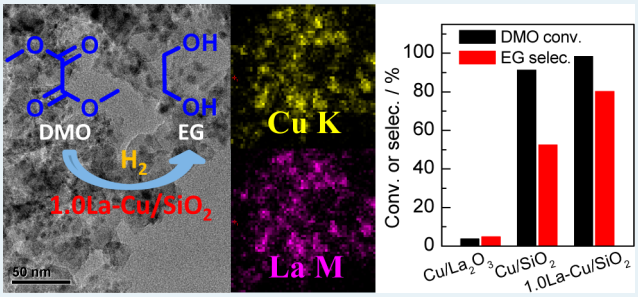

KEYWORDS: *copper, lanthanum oxide, hydrogenation, dimethyl oxalate, ethylene glycol*

1. INTRODUCTION

Ethylene glycol (EG) is an important chemical feedstock used in many industrial processes and has versatile commercial applications.[1] Commercial EG is mainly produced from petroleum-derived ethylene through the hydration of ethylene oxide.[2] Considering the depletion of petroleum resources, an efficient production of EG from syngas through a two-step process consisting of the coupling of CO with nitrite esters to dimethyl oxalate (DMO) and heterogeneous catalytic hydrogenation of DMO to EG is attracting considerable interest.[1−5] However, several problems remain unsolved despite considerable efforts in the study of the DMO hydrogenation process. To date, EG selectivity and catalytic stability still need improvement, the interaction with active sites remains controversial, and the process of catalyst deactivation requires further elucidation. A deeper understanding of the generic concepts is necessary for more rational catalyst design.

Inexpensive Cu-based heterogeneous catalysts are highly active for the chemoselective hydrogenation of DMO to EG.[6−8] Significant advancements in fabricating efficient and stable Cu-based catalysts, as well as the preliminary understanding of the catalytic essence of DMO hydrogenation, have been achieved in the past decade.[2,9−21] Regarding the extensively studied Cu catalyst supported by silica carriers, Cu dispersion and interaction between Cu species and support or promoter are generally believed to be pivotal in determining catalytic activity and stability. Various synthesis methods including ammonia evaporation,[2] urea-assisted precipitation,[22−25] impregnation,[13] and ion-exchange[15] have been successfully developed to produce highly dispersed Cu nanoparticles (NPs) on silica support with high Cu loading. A synergistic effect exists between Cu^0 and Cu^+ species, suggesting the dissociative activation of H_2 molecules on Cu^0 sites as Cu^+ species polarize and activate ester groups in DMO molecules. This phenomenon emphasizes the importance of generating and retaining the appropriate surface distribution of Cu^0 and Cu^+ species during the activation of catalyst precursor and the catalytic operation of DMO hydrogenation.[2,19,22,23,25−29] To improve the poor lifespan of Cu catalyst on silica support mainly ascribed to the agglomeration of Cu NPs and deterioration of metal dispersion during long-term catalytic operation, enhancing the interaction between Cu and its silica support or introducing a promoter to stabilize Cu NPs is considered beneficial. As a weakly acidic carrier, silica poorly interacts with metallic Cu, thereby facilitating the sintering of Cu NPs and the loss of the active cupreous surface as evidenced by the color

Received: July 18, 2013
Revised: October 5, 2013
Published: October 14, 2013

   dx.doi.org/10.1021/cs400574v | ACS Catal. 2013, 3, 2738−2749

change from "gray or black" as a fresh catalyst to "copper red" as a deactivated catalyst.[7,22] From a catalyst precursor with a cupric phyllosilicate phase in which copper atoms are entrapped into a silica network at the atomic level, enhanced metal−support interaction and improved Cu metallic dispersion can be achieved by appropriate thermal reduction activation.

Previous studies on the mechanism of catalytic cycles and catalyst deactivation in Cu-catalyzed DMO hydrogenation indicate that one of the most convenient and feasible means to solve the problems of existing Cu/SiO_2 catalysts in terms of efficiency, stability, and physical property can be achieved by finding appropriate catalyst promoters. Promoters are required to interact appropriately with the Cu component and silica support to generate a fitting and stable catalytic setup. In the case of boric oxide-doped Cu/SiO_2 catalyst, a remarkably prolonged lifespan for DMO hydrogenation into EG or ethanol has been observed, and the strong interaction between boric oxide and surface cupreous species is assumed to be responsible for the stabilizing effect.[22,30] In metallurgy, the rare-earth lanthanum oxide (LaO_x) is sometimes used as an additive to improve the resistance of metal or alloy against sintering, oxidation, corrosion, and wearing.[31] La_2O_3 is also often utilized as a promoter for heterogeneous metal catalysts in various catalytic reactions, such as water−gas shift,[32] syngas methanation,[33] lean-burn NO_x removal,[34] ammonia decomposition,[35] and methane decomposition.[36] The promotional effects of La_2O_3 reportedly originate from several aspects, such as the textural change of catalyst to form special active sites or to increase metal dispersion,[33,34] electronic transfer to decrease the electron density of active metal and stabilize active sites in their appropriate valence state by electron trapping force,[32] and synergistic effect between La-involved sites, as well as other active sites.[35,36] However, the exact nature of the promotional effect of La remains unclear. The introduction of LaO_x into a Cu/SiO_2 catalyst may elicit promotional effects on Cu metallic dispersion to form special surface cupreous species with a thermally stable catalyst structure, among others. Although La_2O_3-supported Cu catalysts are occasionally used for hydrogenation, a detailed study on LaO_x-modified Cu/SiO_2 catalyst systems for DMO hydrogenation has not yet been reported.

In this study, a series of LaO_x-modified Cu/SiO_2 catalysts was designed and fabricated following urea-assisted gelation or impregnation, and their catalytic performances were comprehensively evaluated in the vapor-phase hydrogenation of DMO into EG. Significant improvements in catalytic activity and stability can be achieved by properly controlling the atomic ratio of La/Cu and conducting appropriate activation of the catalyst precursor. To gain further insight on the promotional effect of LaO_x on Cu/SiO_2, a series of catalyst characterizations was performed.

2. EXPERIMENTAL SECTION

2.1. Catalyst Preparation. All catalysts contained a constant, preset Cu loading of 15 wt %. LaO_x-modified Cu/SiO_2-*u* catalysts with various La loadings were prepared by urea-assisted gelation as previously described.[22−25] $Cu(NO_3)_2\cdot 3H_2O$ weighing 4.6 g and a certain amount of $La(NO_3)_3\cdot 6H_2O$ were dissolved in 100 mL of ammonia aqueous solution in a round-bottom flask. Subsequently, 3.0 g of urea was added before slowly dropping 12.0 g of 40 wt % Ludox AS-40 colloidal silica under mechanical stirring. The mixture was vigorously stirred and aged at 343 K in an oil bath for 4 h. The obtained light blue precipitate was separated by high-speed centrifugation, washed three times with deionized water, dried in a vacuum overnight at 393 K, and calcined at 623 K for 2 h in air. The yielded azure powder of catalyst precursor was denoted as *x*La-Cu/SiO_2-*u* (*x* = 0.1, 0.5, 1.0, and 3.0), where *x* is the preset weight percentage of La and *u* represents a synthesis method, i.e., urea-assisted gelation. Cu/SiO_2-*u* catalyst was prepared following the same synthesis procedure for *x*La-Cu/SiO_2-*u* except that no $La(NO_3)_3\cdot 6H_2O$ additive was added. Cu/La_2O_3-*u* catalyst with La_2O_3 as a support was also synthesized by urea-assisted gelation, replacing Ludox AS-40 colloidal silica with an appropriate concentration of aqueous $La(NO_3)_3\cdot 6H_2O$.

For comparison, two La_2O_3-mixed Cu/SiO_2-*u* catalysts were also prepared: one by a synthesis method of postimpregnation, and the other by mechanical mixing. In a typical procedure, a certain quantity of aqueous $La(NO_3)_3\cdot 6H_2O$ solution was added dropwise onto a 100 mL beaker containing Cu/SiO_2-*u* precursor. The obtained slurry was stirred for 12 h at room temperature (RT), dried overnight at 393 K, and calcined for 2 h at 623 K in air, yielding the catalyst precursor denoted as 1.0La-Cu/SiO_2-*i* for the postimpregnation method. Another catalyst denoted as 1.0La-Cu/SiO_2-*m* for mechanical mixing was prepared by mechanically blending $La(NO_3)_3\cdot 6H_2O$ granules and Cu/SiO_2-*u* precursor using a planetary ball mill with agate container and spheres.

2.2. Catalyst Characterization. X-ray diffraction (XRD) patterns of catalysts were collected on a PANalytical X'pert Pro Super X-ray diffractometer using Cu Kα radiation (λ = 0.15418 nm) with a scanning angle (2θ) range of 10° to 90°. The tube voltage and current were 40 kV and 30 mA, respectively. For in situ XRD measurement, the catalyst precursor was placed in a stainless steel holder and covered with a 0.1 mm-thick beryllium plate. A 5% H_2−95% Ar mixture was introduced at a flow rate of 50 mL min^{-1}, and the temperature was ramped from RT to 473, 523, 573, 623, 673, 723, 773, 873, 973, 1073, and 1173 K at a rate of 2 K min^{-1}. The Cu crystallite size was calculated with the Scherrer equation using the full width at half-maximum (fwhm) of the Cu(111) diffraction peak at 2θ = 43.2°.

N_2 adsorption−desorption isotherms were measured by the static volumetric method at 77 K using a Micromeritics TriStar II 3020 surface area and pore analyzer. Before N_2 physisorption measurement, all samples were degassed at 393 K for 1 h and evacuated at 573 K for 3 h to remove physically adsorbed impurities. The specific surface area (S_{BET}) was calculated by the Brunauer−Emmett−Teller (BET) method, adopting isotherm data within the relative pressure (P/P_0) range of 0.05−0.2. The total pore volume (V_p) was derived from the adsorbed N_2 volume at a relative pressure of approximately 0.995, and mesopore size distributions were derived using the desorption branch of isotherm using the Barrett−Joyner−Halenda method.

The H_2 temperature-programmed reduction (H_2-TPR) profiles of the catalysts were measured on a Micromeritics Autochem II 2920 instrument connected with a Hiden Qic-20 mass spectrometry (MS) system. In a typical procedure, 100 mg of catalyst was pretreated at a flow of 20% O_2−80% Ar (50 mL min^{-1}) in a quartz U-tube reactor at 523 K for 1 h. After cooling down to RT in high-purity Ar, a flow of 5% H_2−95% Ar (50 mL min^{-1}) was passed through the catalyst bed. A temperature ramping program from RT to 1073 K at a rate of 5 K min^{-1} was used, and H_2 consumption was monitored with

dx.doi.org/10.1021/cs400574v | ACS Catal. 2013, 3, 2738−2749

MS signals at m/e = 2 in the multiple ion detection (MID) mode.

H_2 temperature-programmed desorption (H_2-TPD) profiles were collected on the same equipment for H_2-TPR measurement. In a typical procedure, 100 mg of catalyst in a quartz U tube was first reduced in 5% H_2−95% Ar at 623 K for 4 h. After the activated catalyst had cooled down to RT, a flow of high-purity H_2 (50 mL min^{-1}) was introduced for 1 h, followed by a purge of high-purity Ar (50 mL min^{-1}) to completely remove unabsorbed H_2 so that the MS signal baseline reached the stable state. Finally, the H_2-TPD profile was collected from RT to 1073 K at a ramping rate of 5 K min^{-1} in a flow of high-purity Ar (50 mL min^{-1}). Desorbed H_2 was monitored with MS signals at m/e = 2 in MID mode.

Transmission electron microscopy (TEM) images were obtained on a TECNAI F-30 transmission electron microscope operating at an acceleration voltage of 300 kV. Elemental distribution in catalyst was determined by energy-dispersive X-ray spectroscopy (EDX) mapping technique in scanning TEM (STEM) mode. To prepare an appropriate sample for TEM observation, catalyst powder was ultrasonically dispersed in ethanol at RT for 30 min and transferred onto carbon-coated copper or molybdenum grid by dipping.

The actual metal contents of catalyst were analyzed by inductively coupled plasma−optical emission spectrometry (ICP-OES) on a Thermo Electron IRIS Intrepid II XSP. The copper surface areas and dispersions of the catalysts were determined on a Micromeritics Autochem II 2920 apparatus with a thermal conductivity detector (TCD) by N_2O chemisorption and H_2 pulse reduction methods based on the stoichiometry of [$2Cu(s) + N_2O \rightarrow Cu_2O(s) + N_2$], where Cu(s) represents surface copper atom.[37] Initially, 100 mg of catalyst precursor was reduced in 5% H_2−95% Ar (50 mL min^{-1}) at 623 K for 4 h and cooled down to 333 K. Pure N_2O (20 mL min^{-1}) was passed through the catalyst bed for 1 h to completely oxidize surface copper atoms into Cu_2O. H_2 pulse reduction was conducted in a flow of high-purity Ar (50 mL min^{-1}) at a temperature of 573 K to guarantee that the chemisorbed oxygen can immediately and thoroughly react with the high-purity H_2 supplied from a 0.4 mL loop. Calibrated TCD was used to quantify the reserved H_2 in the outlet gas in which moisture was removed with a 13 X zeolite dehydration trap. Pulse dosing was repeated at an interval of 3 min until the detected TCD peaks for the latest two or more pulses were constant in the area. The volume of the consumed H_2 was calculated by subtracting the sum of the residual volumes of all unsaturated H_2 pulses from the total H_2 injection volume. Copper dispersion was calculated by dividing the amount of surface copper atom by the total number of supported copper atoms per gram of catalyst. The metallic copper surface area was calculated based on an atomic copper surface density of 1.46×10^{19} Cu atoms m^{-2}.

The Fourier-transform infrared (FT-IR) spectra of catalyst precursors and chemisorbed CO species on activated catalysts were collected on a Nicolet 6700 spectrometer at a special resolution of 4 cm^{-1}. For CO-adsorption experiments, a stainless steel cell with CaF_2 windows and a high-vacuum turbo pump system that allowed in situ thermal treatment up to 873 K under different atmospheres or high vacuum were used. In a typical procedure, 30 mg of catalyst was compressed into a self-supporting wafer and carefully loaded into the in situ cell. The catalyst wafer was reduced for 4 h in a flow of 5% H_2−95% Ar (50 mL min^{-1}) at 623 K and evacuated for 30 min to completely remove chemisorbed surface species. After cooling down to RT, the catalyst wafer was exposed to high-purity CO (760 Torr) for 30 min. IR spectra were collected at different evacuation times and referenced to the background spectrum of 623 K reduced catalyst, which was collected before CO-soaking in a high vacuum at the same temperature.

Characterizations of X-ray photoelectron spectroscopy (XPS) and Auger electron spectroscopy (XAES) were conducted on a Quantum 2000 Scanning ESCA Microprobe instrument (Physical Electronics) equipped with an Al Kα X-ray radiation source ($h\nu$ = 1486.6 eV). The activated catalyst was carefully collected and sealed under the protection of Ar atmosphere after reduction in a flow of 5% H_2−95% Ar at 623 K for 4 h. The collected sample was compressed into a thin disk in a glovebox and transferred to the XPS apparatus analysis chamber. Binding energies were calibrated using the Si 2p peak at 103.7 eV as a reference. Experimental errors were within ±0.2 eV.

2.3. Measurement of Catalytic Activity and Durability. Catalytic evaluation of vapor-phase DMO hydrogenation was conducted in a continuous flow mode using a stainless-steel fixed-bed tubular reactor equipped with a computer-controlled autosampling system. In a typical run, 100 mg of catalyst precursor (40 to 60 meshes) was placed in the center of the reactor (7 mm internal diameter), and the top side of the catalyst bed was packed with adequate quartz powder (40 to 60 meshes). The catalyst was activated in a flow of 5% H_2−95% Ar atmosphere (50 mL min^{-1}) at 623 K for 4 h with a ramping rate of 2 K min^{-1}. The reactor was cooled to the target reaction temperature (443−473 K), and H_2 was fed into the reactor using a mass flow controller. The system pressure was precisely controlled at 3 MPa with a back-pressure regulator. DMO methanol solution (0.02 g mL^{-1}) was pumped into the reactor using a Series III digital HPLC pump (Scientific Systems, Inc.). The outlet stream was sampled using an automatic Valco 6-port valve system and analyzed using an online gas chromatograph (Agilent 7890A) equipped with a flame ionization detector and RTX-Wax capillary column (30 m × 0.25 mm ×0.25 μm) at an interval of 1 h.

3. RESULTS AND DISCUSSION

3.1. Catalyst Crystalline Phase and Morphology. The XRD patterns of Cu/SiO_2-*u*, Cu/La_2O_3-*u*, and *x*La-Cu/SiO_2-*u* catalyst precursors thermally treated in air at 623 K but not subjected to reductive activation with H_2 are shown in Figure 1. No diffraction peak except quite faint ones ascribable to cupric phyllosilicate phases is observed on Cu/SiO_2-*u* and La-Cu/SiO_2-*u* catalysts with <1 wt % La loading. Meanwhile, La loading in La-Cu/SiO_2-*u* catalyst increases to a high level at 3.0 wt %, a series of XRD peaks at 2θ = 17.8°, 24.5°, 30.5°, 43.0°, 43.9°, and 46.9°, which is attributed to lanthanum carbonate hydroxide (JCPDS 00-049-0981),[38] emerges and indicates that urea-assisted gelation enables most species from the $La(NO_3)_3$ precursor to precipitate and mix with Cu/SiO_2 catalyst precursors mainly in the form of lanthanum carbonate hydroxide. For cupric phyllosilicate with low crystallinity at 2θ = 31.0°, 34.8°, 57.2°, 63.3°, and 71.2° (JCPDS 00-003-0219), a series of weak diffraction peaks is present in the XRD patterns of *x*La-Cu/SiO_2-*u* catalyst precursors, indicating that the introduction of $La(NO_3)_3$ into catalyst synthesis systems does not significantly disturb the formation of cupric phyllosilicate, which is believed to be the origin of the high Cu dispersion of Cu/SiO_2-*u* catalyst in urea-assisted gelation.

dx.doi.org/10.1021/cs400574v | ACS Catal. 2013, 3, 2738−2749

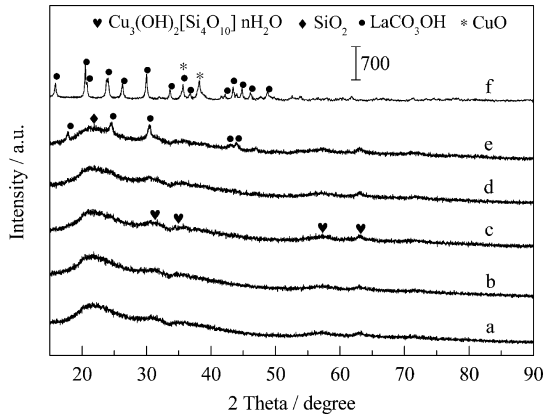

Figure 1. XRD patterns of 623 K-calcined catalyst precursors. (a) Cu/SiO_2-*u*, (b) 0.1La-Cu/SiO_2-*u*, (c) 0.5La-Cu/SiO_2-*u*, (d) 1.0La-Cu/SiO_2-*u*, (e) 3.0La-Cu/SiO_2-*u*, and (f) Cu/La_2O_3-*u*.

FT-IR characterization, which is a useful technique for distinguishing copper phyllosilicate phase, was also adopted.[39] The FT-IR spectra shown in Figure 2 confirm the presence of

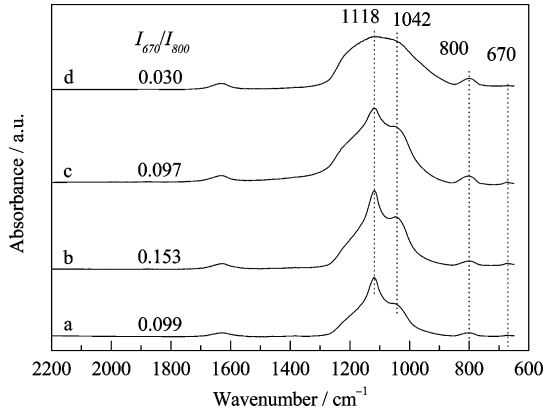

Figure 2. FT-IR spectra of as-calcined catalyst precursors (a) Cu/SiO_2-*u*, (b) 1.0La-Cu/SiO_2-*u*, (c) 1.0La-Cu/SiO_2-*i*, and (d) 1.0La-Cu/SiO_2-*m*. The I_{670}/I_{800} denotes the intensity ratio of two IR bands located at 670 and 800 cm^{-1}.

copper phyllosilicate in *x*La-Cu/SiO_2-*u* catalyst precursors as evidenced by the δ_{OH} band at 670 cm^{-1} and the ν_{SiO} shoulder peak at 1042 cm^{-1}. Because the asymmetric ν_{SiO} band of silica at 1118 cm^{-1} and the ν_{SiO} band of copper phyllosilicate at 1042 cm^{-1} overlap with each other, the relative contents of copper phyllosilicate in different catalysts are compared using the ratio of integrated intensity of δ_{OH} band of copper phyllosilicate at 670 cm^{-1} and symmetric ν_{SiO} band of silica at 800 cm^{-1} denoted as I_{670}/I_{800}.[39] The value of I_{670}/I_{800} for 1.0La-Cu/SiO_2-*u* precursor is 0.153, which is clearly higher than that for Cu/SiO_2-*u* (0.099), 1.0La-Cu/SiO_2-*i* (0.097), and 1.0La-Cu/SiO_2-*m* (0.03). This finding indicates that introducing La species into Cu/SiO_2-*u* by urea-assisted gelation substantially improves the formation of cupric phyllosilicate.

The absence of evident XRD peaks for CuO or other cupreous substances further confirms that Cu atoms are finely dispersed into silica supports by urea-assisted gelation. By contrast, Cu/La_2O_3-*u* catalyst affords two strong diffraction peaks at 2θ = 35.6° and 38.2°, which are characteristic of CuO (JCPDS 01-089-2531). This result signifies that cupreous species are inclined to form copper oxides with relatively large particle sizes from a synthesis system containing urea, $La(NO_3)_3$, and $Cu(NO_3)_2$. Generally, for urea-assisted gelation synthesis in an alkaline environment, silicate anions arising from silica dissolution can react with cuprammonia complexes to form insoluble copper phyllosilicate whiskers.[39] However, under the same environment, no compound like La_2CuO_4 or $CuLa_2O_{4+\delta}$ can be formed from a reaction between copper and lanthanum species. Instead, lanthanum carbonate hydroxide and basic cupric carbonate are preferentially precipitated to form Cu/La_2O_3-*u* catalyst precursor.

For the 1.0La-Cu/SiO_2-*i* catalyst precursor produced by postimpregnation method, the characteristic diffraction peaks of cupreous phyllosilicate seem to be analogous to that with the Cu/SiO_2-*u* catalyst precursor (Supporting Information Figure S1-c), indicating that the introduction of a small quantity of La onto the surface of Cu/SiO_2-*u* and the subsequent thermal treatment at 623 K induces unobvious changes in the crystalline phase of Cu/SiO_2-*u* catalyst. The intensities of the XRD peaks of the cupreous phyllosilicate of 1.0La-Cu/SiO_2-*m* produced by mechanical mixing are weaker than those of Cu/SiO_2-*u*, 1.0La-Cu/SiO_2-*u*, and 1.0La-Cu/SiO_2-*i* catalyst precursors (Supporting Information Figure S1-d) mainly because of the crystallinity deterioration of cupreous phyllosilicate caused by long-time high-energy milling.

In general, metallic Cu NPs highly dispersed in catalyst support tend to be oxidized to cupric oxide (E_{Cu^{2+}/Cu^0} = 0.3419 V) or cuprous oxide (E_{Cu^{+}/Cu^0} = 0.521 V) when exposed to air, even at RT. Thus, in situ XRD was adopted to monitor the phase evolution of Cu/SiO_2-*u*, 1.0La-Cu/SiO_2-*u*, 3.0La-Cu/SiO_2-*u*, and Cu/La_2O_3-*u* catalysts upon reductive activation in 5% H_2−95% Ar atmosphere at different temperatures. For Cu/SiO_2-*u* and 1.0La-Cu/SiO_2-*u* catalysts, the characteristic diffraction peaks for copper phyllosilicate disappear with increased reduction temperature to 523 K (Figures 3A,B).

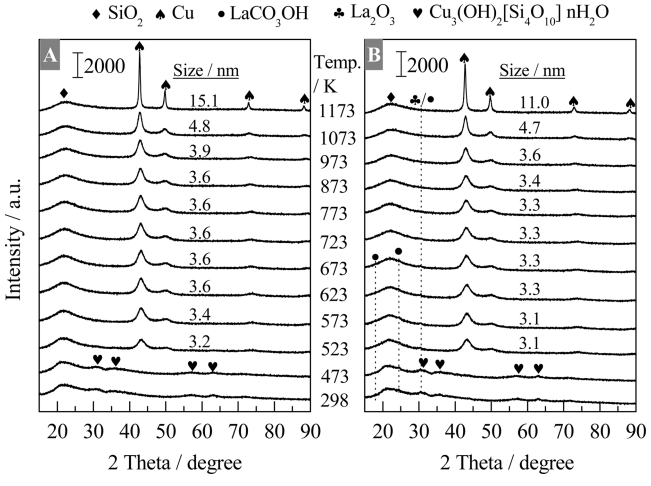

Figure 3. In situ XRD patterns of as-calcined catalysts as a function of the reduction temperature under a 5% H_2−95% Ar atmosphere. (A) Cu/SiO_2-*u* and (B) 1.0La-Cu/SiO_2-*u*.

Moreover, diffraction peaks are observed at 2θ = 43.1°, 50.2°, and 73.9°, which are characteristic of Cu^0 (JCPDS 04-0836). Thus, most Cu^{2+} species entrapped in silica support can be reduced by H_2 at ≤523 K. However, the Cu^{2+} species on the 3.0La-Cu/SiO_2-*u* and Cu/La_2O_3-*u* catalysts are difficultly reduced by H_2 at 523 K. The characteristic Cu^0 diffractions of these two catalysts emerge at a much higher reduction

dx.doi.org/10.1021/cs400574v | ACS Catal. 2013, 3, 2738−2749

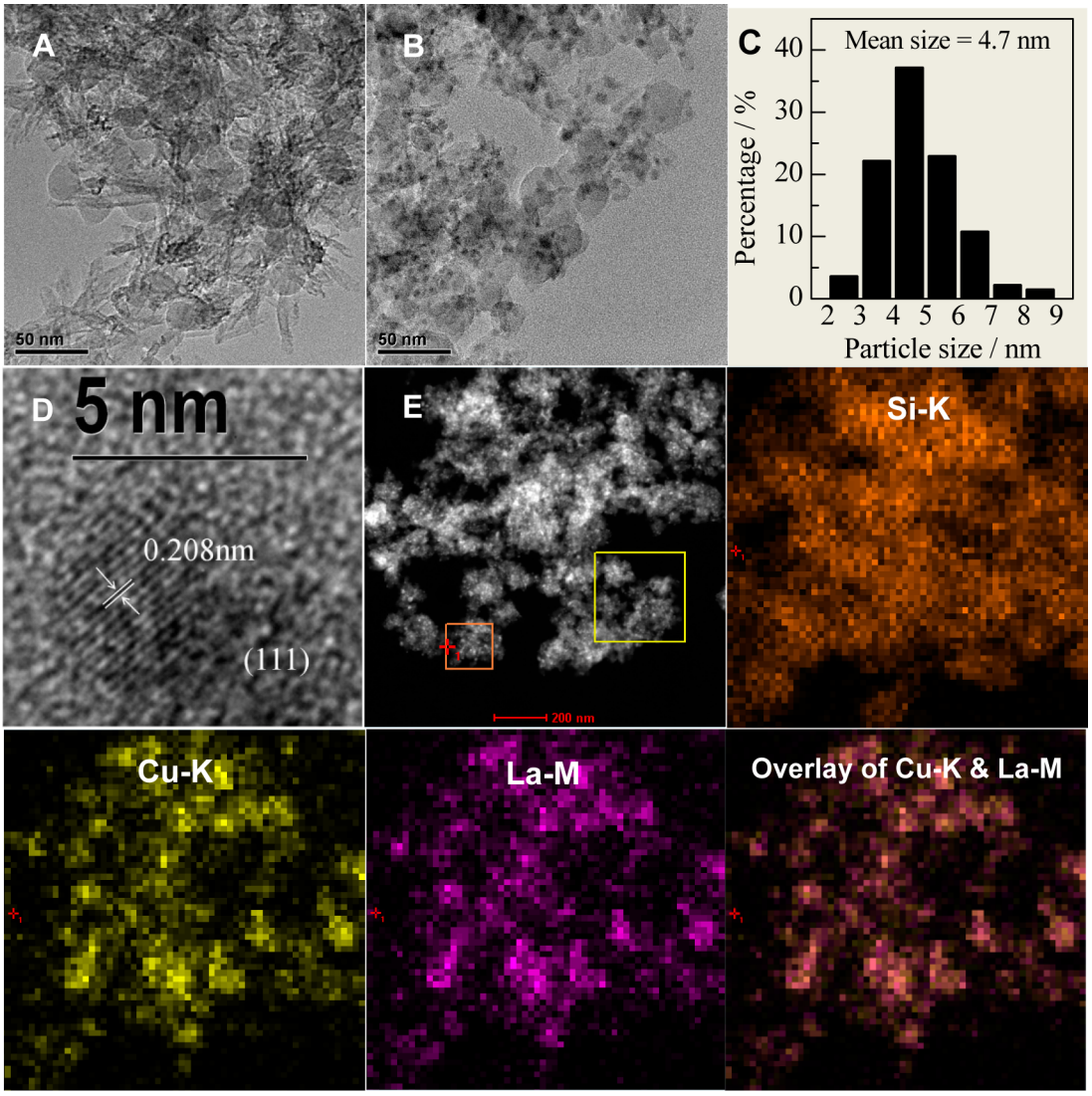

Figure 4. TEM images of 1.0La-Cu/SiO_2-*u*: (A) as-calcined catalyst precursor; (B) as-reduced catalyst; (C) particle size distribution; (D) HRTEM of as-reduced catalyst; (E) HAADF-STEM image of as-reduced catalyst. Elemental EDX maps of as-reduced catalyst corresponded to the orange square region in E. Four maps represent the measured Si K intensity, Cu K intensity, La M intensity, and overlap intensity, respectively.

temperature of 573 and 723 K, respectively (Supporting Information Figure S2). This result strongly indicates that a strong interaction exists between Cu and La species, and this interaction tends to hinder the reduction of Cu^{2+} species to Cu^0. With increased reduction temperature from 523 to 873 K, the diffraction peaks of Cu^0 nanocrystallite on 1.0La-Cu/SiO_2-*u* catalyst does not evidently change, reflecting the relatively high thermal stability of the catalyst. Furthermore, the particle sizes of copper NPs on Cu/SiO_2-*u*, 1.0La-Cu/SiO_2-*u*, and 3.0La-Cu/SiO_2-*u* catalysts were calculated using the Scherrer equation based on the fwhm of the Cu(111) diffraction peak at 2θ = 43.1°, as shown in Figures 3 and Supporting Information Figure S2. Interestingly, the size of copper NPs follows the order Cu/SiO_2-*u* > 1.0La-Cu/SiO_2-*u* > 3.0La-Cu/SiO_2-*u* at almost all treatment temperatures, indicating that the introduction of La species is beneficial for stabilizing small-sized Cu NPs during reductive activation. The diffraction peaks of lanthanum carbonate hydroxide at 2θ = 17.8°, 24.5°, and 30.5° observed on the catalyst precursor Cu/La_2O_3-*u* do not disappear until the temperature increases to 723 K, and the complete transformation to La_2O_3 phase is achieved at a high temperature of 1073 K, indicating the high thermal stability of lanthanum carbonate hydroxide. Meanwhile, highly dispersed lanthanum carbonate hydroxide on 1.0La-Cu/SiO_2-*u* and 3.0La-Cu/SiO_2-*u* catalysts are partly decomposed or reduced to facilitate the high dispersion of lanthanum oxide NPs at a relatively low temperature of 623 K, as evidenced by the weakening of characteristic diffraction peaks. In summary, La species appropriately introduced into Cu/SiO_2-*u* can strongly interact with Cu species on the catalyst precursor to hinder the reduction of Cu^{2+} species to some extent, as well as to retard surface migration and accumulation of nascent Cu^0 NPs into large particles.

The TEM images of the Cu/SiO_2-*u*, 1.0La-Cu/SiO_2-*u*, and 3.0La-Cu/SiO_2-*u* catalyst precursors (Figures 4A and Supporting Information Figure S3) clearly reveal that numerous whisker-shaped copper phyllosilicate particles are present before reductive activation. After reduction at 623 K, only traces of the whisker-shaped copper phyllosilicates remain, and a large number of cross-linked SiO_2 spheres, whose surface is densely covered with black metallic Cu NPs <5 nm in size, are formed. The big rod-shaped particles observed in the TEM

dx.doi.org/10.1021/cs400574v | *ACS Catal.* 2013, 3, 2738−2749

Table 1. Physicochemical Characterization of Several Supported La-Cu/SiO_2 Catalysts

catalyst	Cu loading,[a] wt %	La loading,[a] wt %	S_{BET},[b] $m^2\ g^{-1}$	V_p,[c] $cm^3\ g^{-1}$	D_p,[d] nm	D_{Cu},[e] %	SA_{Cu},[f] $m^2\ g^{-1}$
SiO_2-*u*	–	–	108.2	0.34	9.9	–	–
1.0La/SiO_2-*u*	–	0.84	106.2	0.59	21.1	–	–
Cu/SiO_2-*u*	15.8	0	321.6	0.70	7.5	28.2	28.9
0.1La-Cu/SiO_2-*u*	15.6	0.07	347.9	0.84	7.8	30.9	31.3
0.5La-Cu/SiO_2-*u*	15.3	0.38	342.5	0.73	7.1	32.6	32.4
1.0La-Cu/SiO_2-*u*	15.1	0.77	338.2	0.86	8.4	34.6	33.9
1.0La-Cu/SiO_2-*u*[g]	15.1	0.77	268.8	0.52	7.4	32.1	31.5
3.0La-Cu/SiO_2-*u*	15.8	2.50	334.2	0.79	7.6	29.4	30.1
Cu/La_2O_3-*u*	17.9	70.0	22.4	0.10	20.7	6.2[h]	7.3[h]
1.0La-Cu/SiO_2-*i*	15.2	0.92	307.0	0.70	7.8	26.4	26.0
1.0La-Cu/SiO_2-*m*	15.5	0.86	305.6	0.31	5.0	27.3	27.5

[a]Determined by ICP-OES analysis. [b]BET specific surface area. [c]Pore volume that obtained from $P/P_0 = 0.99$. [d]Pore size. [e]Dispersion of metallic Cu determined by N_2O chemisorption and H_2 pulse reduction. [f]SA_{Cu}: Cu metallic surface area per gram of catalyst. [g]The catalyst was calcined and reduced at 723 K. [h]Determined by TEM images.

image of the Cu/La_2O_3-*u* catalyst precursor are assumed to be lanthanum carbonate hydroxide crystals.[38] Moreover, a number of large, black metallic Cu particles are found after high-temperature reduction at 823 K (Supporting Information Figure S3-c). The mean particle sizes of these Cu particles are approximately consistent with the in situ XRD results for the Cu/SiO_2-*u* and La-Cu/SiO_2-*u* catalysts. In addition, surface characterization by nanoscale elemental STEM-EDX mapping was also used to determine the surface distributions of Cu and La species on the La-Cu/SiO_2-*u* catalysts. The distribution domains of the Cu and La species clearly overlap each other on both nonactivated and reduced catalysts (Figures 4 and Supporting Information Figure S4), demonstrating that via urea-assisted gelation, the La and Cu species are highly dispersed into the silica texture and are in close contact with each other. Moreover, the appropriate reduction activation of La-Cu/SiO_2-*u* catalyst precursors can retain the high dispersion of the La and Cu species. During reductive activation by H_2, some Cu species trapped in the copper phyllosilicate texture undergo gradual reduction into metallic Cu along with electron donation from the activated H-species and tend to aggregate into metallic Cu NPs on the silica support surface. The nascent metallic Cu species act as active sites for H_2 activation to promote the reduction of Cu^{2+} further. Moreover, the partial reduction of La^{3+} into LaO_x, with La in a valence lower than +3, cannot be excluded when neighboring Cu active sites for H_2 activation are abundant.[40] The strong interaction resulting from the close contact between La and Cu species in La−O−Cu bonds can hinder the transformation of the positive-valence Cu species into metallic Cu to some extent.[32,41] Furthermore, as an alkaline metallic oxide, La oxides react with silica to form a La−O−Si silicate phase, which leads to surface modification of the silica support.[42] Thus, the La species introduced into the Cu/SiO_2-*u* catalyst through urea gelation can act as chemical bridges between Cu NPs and the silica surface via La−O−Cu and La−O−Si bonds to enhance metal−support interaction. This enhancement can improve the stability of Cu NPs on the catalyst surface during catalyst activation and catalytic run.

3.2. Physicochemical Properties. The chemical compositions and textural properties of all catalysts are summarized in Table 1. The copper loadings for all catalysts from urea-assisted gelation are close to the preset value of 15 wt %, as determined by ICP-OES. This result is mainly due to the precipitation of most of the Cu species from the $Cu(NO_3)_2$ reagents into copper phyllosilicate during urea-assisted gelation. However, the La contents of these catalysts are slightly lower than the preset values. The N_2 physisorption measurement revealed that the Cu/SiO_2-*u* and *x*La-Cu/SiO_2-*u* catalysts prepared by urea-assisted gelation all exhibit type IV isotherms (Supporting Information Figure S5),[43] which are usually given by mesoporous adsorbents. The shape of hysteresis loop associated with capillary condensation taking place in mesopores is changed to some extent as a result of introducing La species into synthetic system of urea-assisted gelation for Cu/SiO_2-*u* catalysts. The BET surface areas of *x*La-Cu/SiO_2-*u* catalysts ranging from 334.2 $m^2\ g^{-1}$ to 347.9 $m^2\ g^{-1}$ are slightly higher than that of the Cu/SiO_2-*u* catalyst (321.6 $m^2\ g^{-1}$). Moreover, the pore volume of unmodified Cu/SiO_2-*u* catalyst is 0.70 $cm^3\ g^{-1}$ and the introduction of La species increases the pore volumes of *x*La-Cu/SiO_2-*u* catalysts to 0.73−0.86 $cm^3\ g^{-1}$. The different copper phyllosilicate contents in the *x*La-Cu/SiO_2-*u* catalyst precursors, as determined by FTIR characterization (Figure 2), may be responsible for these changes. By contrast, the introduction of La by impregnation and mechanical mixing has a negative effect on the specific surface area of catalyst. The BET surface areas of the 1.0La-Cu/SiO_2-*i* and 1.0La-Cu/SiO_2-*m* catalysts are 307.0 and 305.6 $m^2\ g^{-1}$, respectively, which are all lower than that of the Cu/SiO_2-*u* catalyst (321.6 $m^2\ g^{-1}$). A control experiment on 1.0La-Cu/SiO_2-*u* catalyst using 723 K as calcination/reduction temperature shows decreases in values of S_{BET}, Cu dispersion (D_{Cu}), and Cu metal surface area (SA_{Cu}) (Table 1).

High D_{Cu} and large SA_{Cu} are generally believed to be pivotal in achieving high catalytic activity and stability in chemoselective hydrogenation catalyzed by Cu-based heterogeneous catalysts. The D_{Cu} and SA_{Cu} results as determined by classic N_2O chemisorption are shown in Table 1. La-Cu/SiO_2-*u* catalysts with La loadings below 1 wt % all exhibit higher D_{Cu} and SA_{Cu} values than those of the Cu/SiO_2-*u* catalyst. However, a La loading of 3 wt % results in decreased D_{Cu} and SA_{Cu}. Analogous to the interpretation for the increased BET surface area induced by the introduction of La species via urea-assisted gelation, the larger amount of copper phyllosilicate compounds formed in the *x*La-Cu/SiO_2-*u* catalyst precursors at appropriate La loadings may be the main cause of the improved Cu metal dispersion. The D_{Cu} and SA_{Cu} of 1.0La-Cu/SiO_2-*i* and 1.0La-Cu/SiO_2-*m* are slightly lower than those of the Cu/SiO_2-*u* catalyst, possibly indicating that the direct contact between $La(NO_3)_3$ and copper phyllosilicates in the Cu/SiO_2-*u* catalyst precursor disrupts the mesoporous structure of the Cu/SiO_2-*u*

dx.doi.org/10.1021/cs400574v | ACS Catal. 2013, 3, 2738−2749

catalyst and results in further blockage of some copper surface sites. The low Cu dispersion of the Cu/La_2O_3-*u* catalyst is mainly ascribed to the low porosity and inadequate surface area of the La_2O_3 support, which do not favor the efficient dispersion of the Cu species, particularly for a Cu loading as high as 15 wt %.

3.3. H_2-TPR and H_2-TPD. The effect of the La species on the reducibility of the La-Cu/SiO_2 catalyst precursors was determined using H_2-TPR characterization. The H_2-TPR profiles (Figure 5) show only one H_2 consumption peak over

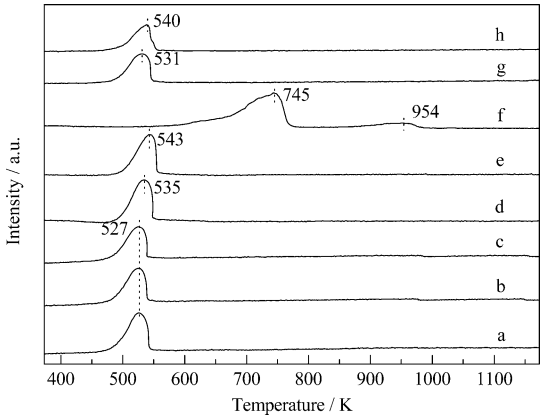

Figure 5. H_2-TPR profiles of as-calcined catalyst precursors. (a) Cu/SiO_2-*u*, (b) 0.1La-Cu/SiO_2-*u*, (c) 0.5La-Cu/SiO_2-*u*, (d) 1.0La-Cu/SiO_2-*u*, (e) 3.0La-Cu/SiO_2-*u*, (f) Cu/La_2O_3-*u*, (g) 1.0La-Cu/SiO_2-*i*, and (h) 1.0La-Cu/SiO_2-*m*.

the Cu/SiO_2-*u* and *x*La-Cu/SiO_2-*u* catalyst precursors. This H_2-TPR peak corresponds to the reduction of the Cu^{2+} species trapped in the silica texture in the form of copper phyllosilicate into metallic Cu. The H_2-TPR peak for the Cu/SiO_2-*u* catalyst precursor is broad and centered at 527 K. Minute amounts (0.1 or 0.5 wt %) of La species introduced into the *x*La-Cu/SiO_2-*u* catalyst precursors appear to have no effect on the reduction behavior of the Cu^{2+} species. As the La loading is increased to 1.0 wt %, the center of the reduction peak slightly shifts from 527 to 535 K. Further increasing the La loading to 3.0 wt % increases the reduction temperature to 543 K. In the in situ XRD characterization under 5% H_2−95% Ar atmosphere, XRD peaks for Cu^0 species emerge at 523 K on Cu/SiO_2-*u* and 1.0La-Cu/SiO_2-*u* catalysts but are only observable at higher temperature (573 K) on 3.0La-Cu/SiO_2-*u* catalyst (Figures 3 and Supporting Information Figure S2-B), also confirming that the introduction of the La species into the Cu/SiO_2-*u* catalyst significantly retards the reduction of the Cu^{2+} species. Two reduction peaks centered at 745 and 954 K, which are significantly higher than the reduction temperature for the Cu/SiO_2-*u* catalyst precursor, are observed on the Cu/La_2O_3-*u* catalyst precursor. This result is consistent with the in situ XRD characterization of the phase evolution of the Cu/La_2O_3-*u* catalyst precursor in a reductive atmosphere (Supporting Information Figure S2−B). In that analysis, the XRD peaks for CuO only disappear after the temperature is increased to 723 K. La_2O_3 reduction by H_2 usually occurs at extremely high temperatures (above 1173 K). However, with the use of metals capable of activating H_2 and supplying active H-species, La_2O_3 may be reduced at relatively low temperatures. For example, Bell and Rieck[40] have observed that lanthanum oxides in the vicinity of Pd NPs can be partially reduced by H_2 at approximately 433 K. For the Cu/La_2O_3-*u* catalyst, the observed reduction peak at 954 K may be ascribed to the partial reduction of the La species, which comes in close contact to the metallic Cu formed by the reduction of Cu^{2+} at low temperatures. The introduction of La species into the Cu/SiO_2-*u* catalyst precursor via the impregnation method also slightly increases the reduction temperature (ca. 531 K) for the 1.0La-Cu/SiO_2-*i* catalyst (Figure 5).

H_2 surface adsorption behaviors on the La-Cu/SiO_2 catalysts were analyzed using the H_2-TPD technique. The H_2-TPD profiles for the Cu/SiO_2-*u* and *x*La-Cu/SiO_2-*u* catalysts, which were activated by H_2 at 623 K for 4 h, all show two desorption peaks located in the 300 to 350 K and 700 to 900 K temperature ranges, respectively (Figure 6). To determine the

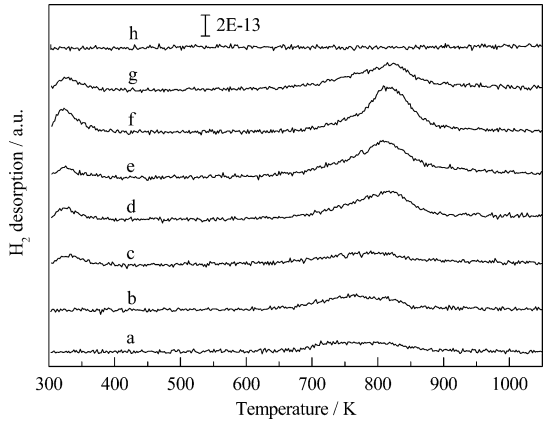

Figure 6. H_2-TPD profiles of as-reduced catalysts. (a) SiO_2, (b) 1.0La/SiO_2-*u*, (c) Cu/SiO_2-*u*, (d) 0.1La-Cu/SiO_2-*u*, (e) 0.5La-Cu/SiO_2-*u*, (f) 1.0La-Cu/SiO_2-*u*, (g) 3.0La-Cu/SiO_2-*u*, and (h) Cu/La_2O_3-*u*.

origins of the two H-adsorption species, a H_2-TPD test was also conducted on a pure silica support. The presence of a weak H_2 desorption peak in the 670 to 900 K range on the H_2-TPD profile for SiO_2 indicates that the observed H_2 desorption at high temperatures corresponds to a number of strongly chemisorbed H_2 species on the silica support surface (Figure 6). Similarly, an investigation by Bettahar et al.[44] on H_2 chemisorption over silica also showed the existence of surface H-species, which were proposed to be formed during the thermal treatment of silica with H_2. Generally, H_2 desorption peaks at low temperature ranges correspond to chemisorbed H_2 on the metallic Cu surface.[45−49] This ascription is supported by appearance of the 323 K H_2 desorption peak only in silica-based catalysts containing Cu. The intensities of the two H_2 desorption peaks of the La-Cu/SiO_2-*u* catalysts are all clearly affected by La loading. As revealed by N_2O chemisorption, the D_{Cu} and SA_{Cu} for the La-Cu/SiO_2-*u* and Cu/SiO_2-*u* catalysts significantly differ even though the actual Cu loadings for these catalysts are nearly identical at ca. 15 wt %. For the 1.0La-Cu/SiO_2-*u* catalyst, which possesses the highest D_{Cu} and SA_{Cu} among all catalysts, the strongest H_2 desorption peaks are located at 323 and 805 K, implying that surface Cu atoms are highly correlated with the formation of the two chemisorbed H-species. However, compared with the unmodified Cu/SiO_2-*u* catalyst, the 3.0La-Cu/SiO_2-*u* catalyst with slightly lower D_{Cu} and SA_{Cu} exhibits the 323 and 805 K H_2 desorption peaks with slightly higher intensities, suggesting that the La species are also involved in H_2 chemisorption and storage on the La-Cu/SiO_2-*u* catalysts. Therefore, the introduction of La species into the Cu/

dx.doi.org/10.1021/cs400574v | ACS Catal. 2013, 3, 2738−2749

SiO_2-*u* catalyst significantly enhances H_2 activation and promotes the surface concentration of the active H-species. These promotional effects may originate from (1) the presence of appropriate La species, which improves the dispersion of Cu atoms trapped in the silica texture and stabilizes the metallic Cu formed by reductive activation in small size, and in turn, the amount of surface metallic Cu atom that can dissociatively activate H_2 molecules and bond with active H-species increases; (2) the appropriate modification of the silica surface by La species, which can increase the number of special adsorption sites capable of strongly chemisorbing H-species; and (3) H_2 spillover or transfer from metallic Cu to the silica support, which is possibly enhanced by a special Cu-LaO_x-SiO_2 interface.

3.4. Chemical States of Surface Species. Prior to XPS measurements, all catalysts were reductively activated by H_2 at 623 K for 4 h. The XPS spectra of Cu 2p (Figure 7) show that,

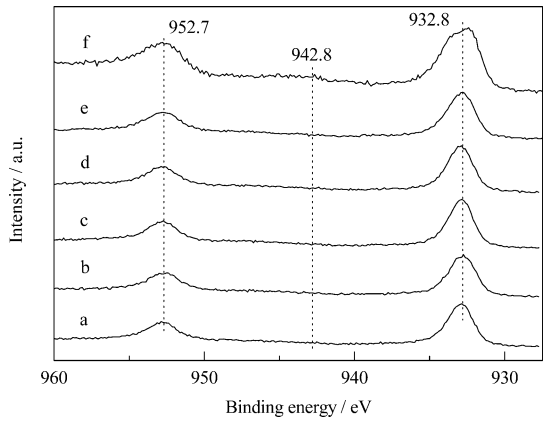

Figure 7. Cu 2p XPS spectra of as-reduced catalysts. (a) Cu/SiO_2-*u*, (b) 0.1La-Cu/SiO_2-*u*, (c) 0.5La-Cu/SiO_2-*u*, (d) 1.0La-Cu/SiO_2-*u*, (e) 3.0La-Cu/SiO_2-*u*, and (f) Cu/La_2O_3-*u*.

over the activated Cu/SiO_2-*u* and *x*La-Cu/SiO_2-*u* catalysts, the Cu $2p_{3/2}$ and Cu $2p_{1/2}$ peaks appear at binding energies of 932.8 and 952.7 eV, respectively. This result suggests that most of the Cu^{2+} species in both the Cu/SiO_2-*u* and the *x*La-Cu/SiO_2-*u* catalyst precursors can be reduced to Cu^0 and/or Cu^+ in the low valence state during reductive activation by H_2 at 623 K because of the absence of a shakeup satellite peak located approximately 10 eV higher than the Cu $2p_{3/2}$ binding energy.[50] On the Cu/La_2O_3-*u* catalyst, a shakeup satellite peak at 942.8 eV, characteristic of the Cu^{2+} species, is observed, confirming that a temperature of 623 K is insufficient to reduce the Cu/La_2O_3-*u* catalyst because of the strong interaction between La and Cu species. This observation is consistent with the H_2-TPR and in situ XRD results. Given that the Cu $2p_{3/2}$ and Cu $2p_{1/2}$ binding energies for Cu^+ and Cu^0 are nearly the same, Cu LMM XAES is usually adopted to discriminate these peaks. A broad, asymmetric Auger kinetic energy peak ranging from 904 to 926 eV is observed on the XAES data for the activated Cu/SiO_2-*u* and *x*La-Cu/SiO_2-*u* catalysts (Figure 8), strongly indicating the simultaneous occurrence of Cu^0 and Cu^+ species on these catalysts. Deconvolution of the Auger kinetic energy peak into two symmetric peaks at ca. 914 and 918 eV, which correspond to Cu^+ and Cu^0, respectively, can help determine the surface distribution of these two species. Deconvolution results (Table 2) show that the proportion of surface Cu^+ species gradually increases with increasing La loading. This result further proves our hypothesis on the existence of a strong

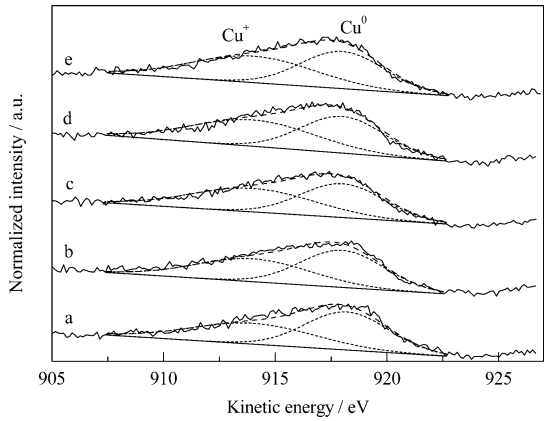

Figure 8. Cu LMM XAES spectra of as-reduced catalysts. (a) Cu/SiO_2-*u*, (b) 0.1La-Cu/SiO_2-*u*, (c) 0.5La-Cu/SiO_2-*u*, (d) 1.0La-Cu/SiO_2-*u*, and (e) 3.0La-Cu/SiO_2-*u*.

Table 2. Deconvolution Results of XPS and Cu LMM XAES of La-Cu/SiO_2 Catalysts

	KE,[a] eV		AP,[b] eV			
catalyst	Cu^+	Cu^0	Cu^+	Cu^0	Cu $2p_{3/2}$ BE, eV	X_{Cu^+},[c] %
Cu/SiO_2-*u*	914.0	918.0	1846.9	1850.9	932.9	46.9
0.1La-Cu /SiO_2-*u*	914.0	918.2	1846.9	1851.1	932.9	49.7
0.5La-Cu /SiO_2-*u*	914.0	918.0	1846.9	1850.9	932.9	51.6
1.0La-Cu /SiO_2-*u*	914.0	918.0	1846.9	1850.9	932.9	54.9
3.0La-Cu /SiO_2-*u*	914.0	918.0	1846.9	1850.9	932.9	56.0

[a]Kinetic energy. [b]Auger parameter. [c]Intensity ratio between Cu^+ and (Cu^+ + Cu^0) by deconvolution of Cu LMM XAES spectra.

interaction between Cu and La species, possibly from the formation of a distinct chemical bond (Cu−O−La). This strong interaction may not only increase the amount of Cu^+ species but also prevent Cu NPs on the catalyst surface from thermally migrating and accumulating.

For the Cu/La_2O_3-*u* catalyst with high La content, the La $3d_{5/2}$ XPS peak at 835.1 eV is attributed to the La^{3+} species (Supporting Information Figure S6). No obvious La $3d_{5/2}$ XPS peak is observed on the *x*La-Cu/SiO_2-*u* (*x* = 0.1, 0.5, 1.0, and 3.0) catalysts, possibly because of the relatively low La loading. Therefore, an accurate determination of the chemical states and surface distribution of the La species is not accomplished. However, the possibility of the existence of partially reduced LaO_x species on the H_2 reduction-activated La-Cu/SiO_2-*u* catalysts could not be excluded.

3.5. In Situ FT-IR Study of CO Chemisorption. FT-IR investigation of CO chemisorption is also useful in distinguishing various surface cupreous species on the supported Cu catalysts. All catalysts were activated by H_2 at 623 K for 4 h prior to CO adsorption at RT for 0.5 h. The FT-IR spectra of the strongly absorbed CO species, which are the reserved species after evacuation for 0.5 h, are shown in Figure 9. The activated La-Cu/SiO_2-*u* catalysts containing La display a significantly stronger IR band at ca. 2120 cm^{-1} compared with that of the unmodified Cu/SiO_2-*u* catalyst. According to literature,[51] the CO species chemisorbed on Cu^+ sites exhibit significantly higher stability than those on Cu^{2+} or Cu^0 sites.

dx.doi.org/10.1021/cs400574v | ACS Catal. 2013, 3, 2738−2749

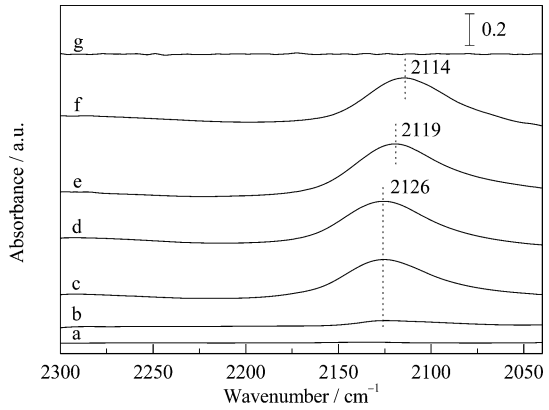

Figure 9. In situ FT-IR spectra of chemisorbed CO on as-reduced catalysts. (a) 1.0La/SiO_2-*u*, (b) Cu/SiO_2-*u*, (c) 0.1La-Cu/SiO_2-*u*, (d) 0.5La-Cu/SiO_2-*u*, (e) 1.0La-Cu/SiO_2-*u*, (f) 3.0La-Cu/SiO_2-*u*, and (g) Cu/La_2O_3-*u*.

Moreover, the IR band for linear CO-Cu^+ usually appears in the 2110 cm^{-1} to 2160 cm^{-1} range. Therefore, this IR band is reasonably ascribed to the linearly bonded CO on the Cu^+ species. Given that the Cu/La_2O_3-*u* catalyst cannot be reduced at 623 K and most of the cupreous species are Cu^{2+}, no strongly chemisorbed CO is observed (Figure 9g). La species seem to be incapable of chemisorbing CO because no observable IR band for chemisorbed CO species can be found on the 1.0La/SiO_2-*u* catalyst (Figure 9a). The La incorporation-induced increase in surface Cu^+ species, as determined by FT-IR characterization of CO chemisorption, is consistent with the aforementioned XAES and XPS results and further confirms our supposition that a strong interaction exists between Cu and La species. In addition, the slight red-shifting of the IR band for the linearly bonded CO on the Cu^+ species as the La loading increases may be due to the effect of the amount of neighboring alkaline LaO_x, which exhibits high electron affinity, on the electron state of the Cu^+ species. Similarly, a previous study by Pestryakov and Davydov[41] showed that the shift in the CO stretching vibration frequency of the reduced CuO/La_2O_3/Al_2O_3 catalyst to the low-frequency range of Cu^+-CO complexes may be due to electronic donor−acceptor interactions of Cu ions with the oxygen ions of La_2O_3.

3.6. Catalytic Activity and Stability. In vapor-phase DMO hydrogenation, a series of successive hydrogenation reactions, including DMO hydrogenation to methyl glycolate (MG), MG hydrogenation to EG, and deep hydrogenation of EG to ethanol, simultaneously occur. A number of reaction factors, including pressure, space velocity, temperature, and relative ratio of substrates, significantly affect catalytic performance. In the present study, an evaluation of the catalytic performance of all catalysts in vapor-phase DMO hydrogenation was conducted under identical conditions: 453 K, 3.0 MPa, DMO weight liquid hourly space velocity ($WLHSV_{DMO}$) = 0.5 g g_{-cat}^{-1} h^{-1} to 3.5 g g_{-cat}^{-1} h^{-1}, and H_2/DMO = 80. At a low $WLHSV_{DMO}$ of 1.5 g g_{-cat}^{-1} h^{-1}, Cu/SiO_2-*u* and most of the La-Cu/SiO_2-*u* catalysts display high hydrogenation activity, with a DMO conversion above 90% (Table 3). Increasing the $WLHSV_{DMO}$ to 3.5 g g_{-cat}^{-1} h^{-1} results in a significant decrease in DMO conversion. However, a DMO conversion of 69.2% can still be obtained over the optimum 1.0La-Cu/SiO_2-*u* catalyst (Figure 10). The La loading clearly affects the catalytic activity and EG selectivity, which follows the order 1.0La-Cu/SiO_2-*u* > 0.5La-Cu/SiO_2-*u* > 0.1La-Cu/SiO_2-*u* > Cu/SiO_2-*u* > 3.0La-Cu/SiO_2-*u* (Table 3). Apparently, the introduction of La species into the Cu/SiO_2-*u* catalyst within the appropriate content range significantly improves in the catalytic performance of the Cu/SiO_2-*u* catalyst for DMO hydrogenation. The 1.0La-Cu/SiO_2-*i* catalyst from the impregnation method also shows superior DMO conversion (96.6%) and EG selectivity (65.5%) compared with those of the Cu/SiO_2-*u* catalyst, further confirming that the La species promote the DMO hydrogenation activity of the Cu/SiO_2 catalyst. The low catalytic performance of the 1.0La-Cu/SiO_2-*m* catalyst from the mechanical mixing method may be due to the serious damage on the Cu/SiO_2-*u* catalyst precursor structure induced by the long, high-energy milling treatment. This damage was revealed by XRD and static N_2-physisorption characterizations.

Table 3. Performance of Vapor-Phase Chemoselective Hydrogenation of DMO to EG over La-Cu/SiO_2 Catalysts[a]

		selec., %			
catalyst	conv., %	EG	MG	others[b]	STY_{EG},[c] g g_{-cat}^{-1} h^{-1}
1.0La/SiO_2-*u*	0.3	5.5	94.5	0.0	0.00
Cu/SiO_2-*u*	91.3	52.5	47.3	0.3	0.38
0.1La-Cu/SiO_2-*u*	97.4	60.1	39.5	0.5	0.46
0.5La-Cu/SiO_2-*u*	97.9	76.3	22.4	1.3	0.59
1.0La-Cu/SiO_2-*u*	98.5	80.3	17.6	2.2	0.62
1.0La-Cu/SiO_2-*u*[d]	96.9	67.8	31.2	1.0	0.52
3.0La-Cu/SiO_2-*u*	79.5	23.2	76.7	0.1	0.14
Cu/La_2O_3-*u*	3.8	4.8	95.2	0.0	0.00
1.0La-Cu/SiO_2-*i*	96.6	65.5	33.8	0.7	0.50
1.0La-Cu/SiO_2-*m*	25.9	30.3	69.5	0.0	0.05

[a]Reaction conditions: T = 453 K, $P(H_2)$ = 3.0 MPa, H_2/DMO = 80, $WLHSV_{DMO}$ = 1.5 g g_{-cat}^{-1} h^{-1}. [b]Others include EtOH, 1,2-BDO, and 1,2-PDO. [c]STY_{EG} represents the space time yield of EG for the fresh catalysts, gram of EG per gram of catalyst per hour (g g_{-cat}^{-1} h^{-1}). [d]The catalyst was calcined and reduced at 723 K.

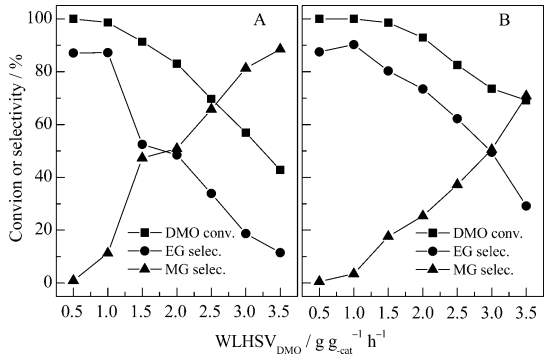

Figure 10. DMO hydrogenation over (A) Cu/SiO_2-*u* and (B) 1.0La-Cu/SiO_2-*u* catalysts as a function of $WLHSV_{DMO}$. Reaction conditions: T = 453 K, $P(H_2)$ = 3.0 MPa, H_2/DMO = 80.

In general, high metal dispersion is assumed to promote the hydrogenation activity of Cu/SiO_2 catalysts,[16,52] which can be affected by several parameters like promoters/additives and pretreatment conditions. The control experiments on 1.0La-Cu/SiO_2-*u* catalyst using 723 K (presumably converting $LaCO_3OH$ to La_2O_3) as calcination/reduction temperature show drops in S_{BET}, SA_{cu}, and lower activity (Tables 1, 3, and 4), probably indicating that the La species formed at 623 K may be better and the sintering of Cu NPs may occur under higher treatment temperatures. The measured D_{Cu} for the different catalysts listed in Table 1 appear to correlate well with their

dx.doi.org/10.1021/cs400574v | ACS Catal. 2013, 3, 2738−2749

Table 4. TOF of La-Cu/SiO_2 Catalysts for the Vapor-Phase Chemoselective Hydrogenation of DMO to EG[a]

catalyst	$WLHSV_{DMO}$, g g_{-cat}^{-1} h^{-1}	conv., %	selec., % EG	MG	others[b]	TOF,[c] h^{-1}
Cu/SiO_2-*u*	4.0	13.3	7.4	92.6	0.0	6.4
0.1La-Cu/SiO_2-*u*	4.0	22.7	11.3	88.7	0.0	10.1
0.5La-Cu/SiO_2-*u*	5.0	23.6	15.2	84.8	0.0	12.7
1.0La-Cu/SiO_2-*u*	6.0	28.5	22.7	77.2	0.1	17.6
1.0La-Cu/SiO_2-*u*[d]	4.5	24.9	16.1	83.9	0.0	12.4
3.0La-Cu/SiO_2-*u*	4.0	3.6	2.3	97.7	0.0	2.1
Cu/La_2O_3-*u*	1.5	3.8	4.8	95.2	0.0	2.8
1.0La-Cu/SiO_2-*i*	4.0	26.5	13.0	87.0	0.0	14.2
1.0La-Cu/SiO_2-*m*	1.5	25.9	30.3	69.5	0.0	4.9

[a]Reaction conditions: T = 453 K, $P(H_2)$ = 3.0 MPa, H_2/DMO = 80. [b]Others include EtOH, 1,2-BDO and 1,2-PDO. [c]TOF values were calculated according to the Cu dispersion in Table 1. [d]The catalyst was calcined and reduced at 723 K.

hydrogenation activities. However, the catalytic activity is not simply determined by the amount of surface metallic Cu atoms because the TOF values for the Cu/SiO_2-*u* and *x*La-Cu/SiO_2-*u* catalysts significantly change with the La loading (Table 4). The optimal 1.0La-Cu/SiO_2-*u* catalyst with the highest DMO hydrogenation performance possesses a TOF of 17.6 h^{-1}, which is significantly higher than that of unmodified Cu/SiO_2-*u* (6.4 h^{-1}). This result strongly suggests that the catalytic cycles of vapor-phase DMO hydrogenation are not related exclusively to the surface Cu^0 sites. For the vapor-phase DMO hydrogenation catalyzed with heterogeneous Cu-based catalysts, surface adsorption and activation on the catalytic sites of substrates and of reaction intermediates, including H_2, DMO, and MG molecules, as well as the surface reactions of the activated species, are all vital catalytic steps. To date, although the catalytic mechanism of DMO hydrogenation remains unclear, a number of assumptions have been preliminarily proposed to interpret the complicated hydrogenation behaviors of Cu-based catalysts. For example, Chen et al.[2] suggested that H_2 dissociative activation on Cu^0 surfaces and the C═O bond in DMO molecules are polarized and activated on Cu^+ sites. As can be seen from Table 1, the measurement of N_2O chemisorption reveals that the values of D_{Cu} and SA_{Cu} tend to increase when an appropriate La amount is introduced into the Cu/SiO_2-*u* catalysts by urea-assisted gelation. From the deconvolution results of Cu LMM XAES listed in Table 2, the X_{Cu^+} ratio (X_{Cu^+} = $Cu^+/(Cu^+ + Cu^0)$) also increases with the increase of La addition. Combining the results of N_2O chemisorption and XPS, we can make an estimation on the amounts of surface Cu^0 and Cu^+ sites. The results show that the amounts of Cu^+ and Cu^0 sites on the La-free Cu/SiO_2-*u* catalyst are about 13.6 m^2 g^{-1} and 15.3 m^2 g^{-1}, respectively. When 0.1 wt % La is added, the amounts of Cu^+ and Cu^0 sites on the 0.1La-Cu/SiO_2-*u* catalyst increase to 15.6 m^2 g^{-1} and 15.7 m^2 g^{-1}, respecively. We consider that the increases are mainly resulted from increases of D_{Cu} and SA_{Cu} and the strong interactions between the La and Cu species. When the La addtion is increased to 1.0 wt %, there is only a gradual increase in the amount of Cu^+ site associated with almost no changes in that of the Cu^0 one. Further increase of La amount to 3.0 wt % will cause drops in the amounts of both Cu^+ and Cu^0 sites, probably due to the blockage of La species. Therefore, the increased catalytic activity for DMO hydrogenation may be mainly ascribed to the surface concentrations of active sites for both H_2 and DMO molecule activation, which are assumed to be Cu^0 and Cu^+ sites, respectively. The H_2-TPD results clearly prove that the concentrations of two types of chemisorbed H-species all reach the maximum on the most active 1.0La-Cu/SiO_2-*u* catalyst. With respect to the Cu^+ catalytic sites for DMO activation, the cupreous species located at the interface between Cu NPs and the catalyst support are likely stabilized in the +1 valence state as a result of the electron donor−acceptor transfer between interfacial Cu atoms and the adjacent oxygen atoms of the oxide support.[32,41] On the basis of this hypothesis, the chemical state of the Cu^+ species on the Cu/SiO_2-*u* catalyst may be quite different from that on the La-Cu/SiO_2-*u* catalyst because of the existence of a strong interaction between adjacent Cu and La species, as confirmed by H_2-TPR and in situ XRD characterizations. Therefore, the difference between the chemical states of the Cu^+ species on the Cu/SiO_2-*u* and La-Cu/SiO_2-*u* catalysts may be partially responsible for their significantly dissimilar TOFs for DMO catalytic hydrogenation.

To date, the high deactivation and inadequate lifespan of Cu-based hydrogenation catalysts remain significant problems that hinder the practical industrialization of vapor-phase hydrogenation of DMO to EG. The long-term catalytic performances of the optimal 1.0La-Cu/SiO_2-*u* and unmodified Cu/SiO_2-*u* catalysts were compared under conventional reaction conditions, namely, 473 K, 3.0 MPa, H_2/DMO = 80, and $WLHSV_{DMO}$ = 1.5 g g_{-cat}^{-1} h^{-1} (Figure 11). The 1.0La-Cu/SiO_2-*u* catalyst retains its high catalytic activity, with no significant changes, during DMO hydrogenation for 200 h. On the other hand, the unmodified Cu/SiO_2-*u* catalyst is clearly deactivated within 80 h. These results indicate the superior catalytic stability of the modified catalyst for long-term hydrogenation operations. In general, Cu sintering induced by thermal surface mass transfers, structural collapse, or erosion of the catalyst support is believed to be the main cause of catalyst deactivation.[53,54] The Cu/SiO_2-*u* catalyst seems to be quite stable within the first 45 h on stream but suddenly lost its

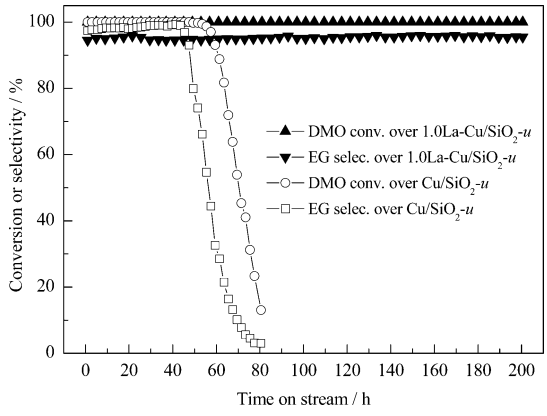

Figure 11. DMO hydrogenation over Cu/SiO_2-*u* and 1.0La-Cu/SiO_2-*u* catalysts as a function of time on stream. Reaction conditions: T = 473 K, $P(H_2)$ = 3.0 MPa, H_2/DMO = 80, $WLHSV_{DMO}$ = 1.5 g g_{-cat}^{-1} h^{-1}.

dx.doi.org/10.1021/cs400574v | ACS Catal. 2013, 3, 2738−2749

catalytic activity in relatively short time (from 50 to 80 h). We have repeated the experiment several times, and the sharp deactivation is always observed. Among possible causes for catalyst deactivation, catalyst poisoning and blocking of active sites by carbon deposit could be excluded since the regeneration of deactivated catalyst by calcination and rereduction did not restore the catalytic activity. It is found that the Cu particle size of Cu/SiO_2-*u* increased obviously after the serious catalyst deactivation. Therefore we would like to ascribe the main cause for catalyst deactivation to the deterioration of Cu dispersion. However, the growth of Cu particles during catalytic operation of DMO hydrogenation should be a continuous and gradual process, which is unlikely to induce the sharp decay of catalytic activity. As we know, the synergistic effect between Cu^0 and Cu^+ species exists in catalytic hydrogenation of DMO. The Cu^0 sites activate H_2 molecules and Cu^+ species polarize and activate the ester groups of DMO molecules. Thus, we speculate that the size of Cu particles and the strength of interaction between metal and support can greatly influence the surface distribution of Cu^0 and Cu^+ species. For the Cu^+ species, which possibly locate in the interface between Cu particles and SiO_2 support, the amount may significantly decrease when the growth of Cu particle exceeds a special extent due to the obvious change of interfacial state. This and other results likewise demonstrate that the hydrogenation of DMO is a structure-sensitive reaction.[22,25] Therefore, the decrease of surface cupreous species and the serious destruction of synergetic catalysis between Cu^0 and Cu^+ active sites can lead to the sharp decay in catalytic activity. The considerably enhanced catalytic stability of the 1.0La-Cu/SiO_2-*u* catalyst may be ascribed to the stabilizing effect of the La species on the surface cupreous species via strong interaction or bonding between them.

4. CONCLUSIONS

The catalytic behaviors of vapor-phase, chemoselective hydrogenation of DMO over a series of La-modified Cu/SiO_2 catalysts were investigated. Marked improvements in both hydrogenation activity and catalytic stability were observed after introduction of a La promoter. The 1.0La-Cu/SiO_2-*u* catalyst prepared by urea-assisted gelation and which has a low La loading of 1 wt % displayed the highest catalytic performance. The existence of strong interactions between the La promoters and the Cu species was deduced from H_2-TPR and in situ XRD results. N_2O chemisorption and H_2-TPD characterizations further showed that the metallic dispersion of Cu and surface concentration of chemisorbed H-species were all enhanced by the introduction of La promoters into the Cu/SiO_2 catalyst. In addition, the amount of surface Cu^+ species, which are assumed to be involved in the activation of DMO molecules, also increased, as confirmed by X-ray Auger electron spectroscopy and in situ FT-IR of chemisorbed CO. The formation of distinct Cu−O−La bonds between LaO_x and the cupreous species located at interfacial sites may be responsible for the significantly improved catalytic performance and stability.

■ ASSOCIATED CONTENT

Supporting Information

XRD, in situ XRD, HAADF-STEM images, elemental EDX maps, and La 3d XPS spectra of some catalysts. This material is available free of charge via the Internet at http://pubs.acs.org.

■ AUTHOR INFORMATION

Corresponding Authors

*(H.L.) Phone: +86-592-2182287. Fax: +86 592 2182287. E-mail: hqlin@xmu.edu.cn.

*(Y.Y.) Phone: +86-592-2181659. Fax: +86 592 2183047. E-mail: yzyuan@xmu.edu.cn.

Notes

The authors declare no competing financial interest.

■ ACKNOWLEDGMENTS

We gratefully acknowledge the financial support from the National Basic Research Program of China (2011CBA00508), the Natural Science Foundation of China (21173175 and 20923004), the Research Fund for the Doctoral Program of Higher Education (20110121130002), and the Program for Changjiang Scholars and Innovative Research Team in University (IRT1036).

■ REFERENCES

(1) Yue, H. R.; Zhao, Y. J.; Ma, X. B.; Gong, J. L. *Chem. Soc. Rev.* **2012**, *41*, 4218−4244.

(2) Chen, L. F.; Guo, P. J.; Qiao, M. H.; Yan, S. R.; Li, H. X.; Shen, W.; Xu, H. L.; Fan, K. N. *J. Catal.* **2008**, *257*, 172−180.

(3) Kerr, R. A.; Service, R. F. *Science* **2005**, *309*, 101.

(4) Xu, G. H.; Li, Y. C.; Li, Z. H.; Wang, H. J. *Ind. Eng. Chem. Res.* **1995**, *34*, 2371−2378.

(5) Xu, Z. N.; Sun, J.; Lin, C. S.; Jiang, X. M.; Chen, Q. S.; Peng, S. Y.; Wang, M. S.; Guo, G. C. *ACS Catal.* **2013**, *3*, 118−122.

(6) Brands, D. S.; Poels, E. K.; Bliek, A. *Appl. Catal., A* **1999**, *184*, 279−289.

(7) Wall, R. G. U.S. Patent 4,149,021, 1979.

(8) Bartley, W. J. U.S. Patent 4,628,128, 1986.

(9) Lin, L.; Pan, P. B.; Zhou, Z. F.; Li, Z. J.; Yang, J. X.; Sun, M. L.; Yao, Y. G. *Chin. J. Catal.* **2011**, *32*, 957−969.

(10) Wang, S. R.; Li, X. B.; Yin, Q. Q.; Zhu, L. J.; Luo, Z. Y. *Catal. Commun.* **2011**, *12*, 1246−1250.

(11) Yin, A. Y.; Guo, X. Y.; Dai, W. L.; Fan, K. N. *Acta Chim. Sin.* **2009**, *67*, 1731−1736.

(12) Yin, A. Y.; Guo, X. Y.; Dai, W. L.; Fan, K. N. *J. Phys. Chem. C* **2010**, *114*, 8523−8532.

(13) Yin, A. Y.; Guo, X. Y.; Dai, W. L.; Li, H. X.; Fan, K. N. *Appl. Catal., A* **2008**, *349*, 91−99.

(14) Li, Z. X.; Qian, Z. G.; Zhao, X. G.; Xiao, W. D. *Chem. React. Eng. Technol.* **2004**, *20*, 121−128.

(15) Yin, A. Y.; Guo, X. Y.; Fan, K. N.; Dai, W. L. *ChemCatChem* **2010**, *2*, 206−213.

(16) Zhu, Y. Y.; Wang, S. R.; Zhu, L. J.; Ge, X. L.; Li, X. B.; Luo, Z. Y. *Catal. Lett.* **2010**, *135*, 275−281.

(17) Zhao, L.; Zhao, Y. J.; Wang, S. P.; Yue, H. R.; Wang, B.; Lv, J.; Ma, X. B. *Ind. Eng. Chem. Res.* **2012**, *51*, 13935−13943.

(18) Yue, H. R.; Zhao, Y. J.; Zhao, L.; Lv, J.; Wang, S. P.; Gong, J. L.; Ma, X. B. *AIChE J.* **2012**, *58*, 2798−2809.

(19) Gong, J. L.; Yue, H. R.; Zhao, Y. J.; Zhao, S.; Zhao, L.; Lv, J.; Wang, S. P.; Ma, X. B. *J. Am. Chem. Soc.* **2012**, *134*, 13922−13925.

(20) Yin, A. Y.; Guo, X. Y.; Dai, W. L.; Fan, K. N. *J. Phys. Chem. C* **2009**, *113*, 11003−11013.

(21) Wen, C.; Cui, Y. Y.; Yin, A. Y.; Fan, K. N.; Dai, W. L. *ChemCatChem* **2013**, *5*, 138−141.

(22) He, Z.; Lin, H. Q.; He, P.; Yuan, Y. Z. *J. Catal.* **2011**, *277*, 54−63.

(23) Lin, H. Q.; Zheng, X. L.; He, Z.; Zheng, J. W.; Duan, X. P.; Yuan, Y. Z. *Appl. Catal., A* **2012**, *445*−*446*, 287−296.

(24) Lin, H. Q.; Duan, X. P.; Zheng, J. W.; Zheng, X. L.; He, P.; Yuan, Y. Z.; Yang, Y. H. *RSC Adv.* **2013**, *3*, 11782−11789.

(25) Huang, Y.; Ariga, H.; Zheng, X. L.; Duan, X. P.; Takakusagi, S.; Asakura, K.; Yuan, Y. Z. *J. Catal.* **2013**, *307*, 74−83.

(26) Monnier, J. R.; Hanrahan, M. J.; Apai, G. *J. Catal.* **1985**, *92*, 119−126.
(27) Rao, R.; Dandekar, A.; Baker, R. T. K.; Vannice, M. A. *J. Catal.* **1997**, *171*, 406−419.
(28) Sitthisa, S.; Sooknoi, T.; Ma, Y. G.; Balbuena, P. B.; Resasco, D. E. *J. Catal.* **2011**, *277*, 1−13.
(29) Wang, Y. N.; Duan, X. P.; Zheng, J. W.; Lin, H. Q.; Yuan, Y. Z.; Ariga, H.; Takakusagi, S.; Asakura, K. *Catal. Sci. Technol.* **2012**, *2*, 1637−1639.
(30) Zhao, S.; Yue, H. R.; Zhao, Y. J.; Wang, B.; Geng, Y. C.; Lv, J.; Wang, S. P.; Gong, J. L.; Ma, X. B. *J. Catal.* **2013**, *297*, 142−150.
(31) Zhou, Y. F.; Yang, Y. L.; Qi, X. W.; Jiang, Y. W.; Yang, J.; Ren, X. J.; Yang, Q. X. *J. Rare Earths* **2012**, *30*, 1069−1074.
(32) Kam, R.; Selomulya, C.; Amal, R.; Scott, J. *J. Catal.* **2010**, *273*, 73−81.
(33) Kok, E.; Scott, J.; Cant, N.; Trimm, D. *Catal. Today* **2011**, *164*, 297−301.
(34) Ozawa, M.; Toda, H.; Suzuki, S. *Appl. Catal., B* **1996**, *8*, 141−155.
(35) Liu, H. C.; Wang, H.; Shen, J. H.; Sun, Y.; Liu, Z. M. *Catal. Today* **2008**, *131*, 444−449.
(36) Cunha, A. F.; Mahata, N.; Órfão, J. J. M.; Figueiredo, J. L. *Energy Fuel* **2009**, *23*, 4047−4050.
(37) Dandekar, A.; Vannice, M. A. *J. Catal.* **1998**, *178*, 621−639.
(38) Li, G. G.; Shang, M. M.; Geng, D. L.; Yang, D. M.; Peng, C.; Cheng, Z. Y.; Lin, J. *CrystEngComm* **2012**, *14*, 2100−2111.
(39) Toupance, T.; Kermarec, M.; Lambert, J. F.; Louis, C. *J. Phys. Chem. B* **2002**, *106*, 2277−2286.
(40) Rieck, J. S.; Bell, A. T. *J. Catal.* **1985**, *96*, 88−105.
(41) Pestryakov, A. N.; Davydov, A. A. *Appl. Surf. Sci.* **1996**, *103*, 479−483.
(42) Vidal, H.; Bernal, S.; Baker, R. T.; Finol, D.; Omil, J. A. P.; Pintado, J. M.; Rodríguez-Izquierdo, J. M. *J. Catal.* **1999**, *183*, 53−62.
(43) Sing, K. S. W.; Everett, D. H.; Haul, R. A. W.; Moscou, L.; Pierotti, R. A.; Rouquérol, J.; Siemieniewska, T. *Pure Appl. Chem.* **1985**, *57*, 603−619.
(44) Boudjahem, A. G.; Monteverdi, S.; Mercy, M.; Ghanbaja, D.; Bettahar, M. *Catal. Lett.* **2002**, *84*, 115−122.
(45) Wilmer, H.; Genger, T.; Hinrichsen, O. *J. Catal.* **2003**, *215*, 188−198.
(46) Waugh, K. C. *Solid State Ionics* **2004**, *168*, 327−342.
(47) Ahlers, J. A.; Grasser, J. A.; Loveless, B. T.; Muggli, D. S. *Catal. Lett.* **2007**, *114*, 185−191.
(48) Genger, T.; Hinrichsen, O.; Muhler, M. *Catal. Lett.* **1999**, *59*, 137−141.
(49) Dong, X.; Zhang, H. B.; Lin, G. D.; Yuan, Y. Z.; Tsai, K. R. *Catal. Lett.* **2003**, *85*, 237−246.
(50) Kim, K. S. *J. Electron Spectrosc.* **1974**, *3*, 217−226.
(51) Hadjiivanov, K.; Knozinger, H. *Phys. Chem. Chem. Phys.* **2001**, *3*, 1132−1137.
(52) Lambert, S.; Cellier, C.; Grange, P.; Pirard, J. P.; Heinrichs, B. *J. Catal.* **2004**, *221*, 335−346.
(53) Lin, J. D.; Zhao, X. Q.; Cui, Y. H.; Zhang, H. B.; Liao, D. W. *Chem. Commun.* **2012**, *48*, 1177−1179.
(54) Wen, C.; Cui, Y. Y.; Dai, W. L.; Xie, S. H.; Fan, K. N. *Chem. Commun.* **2013**, *49*, 5195−5197.